

A Novel Supervised Approach for Segmentation of Lung Parenchyma from Chest CT for Computer-Aided Diagnosis

Shiloah Elizabeth Darmanayagam ·
Khanna Nehemiah Harichandran ·
Sunil Retmin Raj Cyril · Kannan Arputharaj

Published online: 18 October 2012
© Society for Imaging Informatics in Medicine 2012

Abstract Segmentation of lung parenchyma from the chest computed tomography is an important task in analysis of chest computed tomography for diagnosis of lung disorders. It is a challenging task especially in the presence of peripherally placed pathology bearing regions. In this work, we propose a segmentation approach to segment lung parenchyma from chest. The first step is to segment the lungs using iterative thresholding followed by morphological operations. If the two lungs are not separated, the lung junction and its neighborhood are identified and local thresholding is applied. The second step is to extract shape features of the two lungs. The third step is to use a multilayer feed forward neural network to determine if the segmented lung parenchyma is complete, based on the extracted features. The final step is to reconstruct the two lungs in case of incomplete segmentation, by exploiting the fact that in majority of the cases, at least one of the two

lungs would have been segmented correctly by the first step. Hence, the complete lung is determined based on the shape and region properties and the incomplete lung is reconstructed by applying graphical methods, namely, reflection and translation. The proposed approach has been tested in a computer-aided diagnosis system for diagnosis of lung disorders, namely, bronchiectasis, tuberculosis, and pneumonia. An accuracy of 97.37 % has been achieved by the proposed approach whereas the conventional thresholding approach was unable to detect peripheral pathology-bearing regions. The results obtained prove to be better than that achieved using conventional thresholding and morphological operations.

Keywords Segmentation · Lung parenchyma · Chest CT · Thresholding · Morphological operations · Multilayer feed forward neural network

S. E. Darmanayagam
Department of Computer Science and Engineering,
Anna University,
Chennai 600 025, Tamilnadu, India

S. E. Darmanayagam
e-mail: shiloah@cs.annauniv.edu

K. N. Harichandran (✉) · S. R. R. Cyril
Ramanujan Computing Centre, Anna University,
Chennai 600 025, Tamilnadu, India
e-mail: nehemiah@annauniv.edu

K. N. Harichandran
e-mail: harikhanna@hotmail.com

S. R. R. Cyril
e-mail: retmin2001@gmail.com

K. Arputharaj
Department of Information Science and Technology,
Anna University,
Chennai 600 025, Tamilnadu, India

K. Arputharaj
e-mail: kannan@annauniv.edu

Introduction

Lung disorders are threatening the health of individuals all over the world especially in South-East Asia. According to a WHO report [1], an estimated 1.3 million people died from tuberculosis in 2008; the highest number of deaths was in South-East Asia and the number of new cases arising each year is still increasing globally in the WHO regions of Africa, the East Mediterranean, and South-East Asia. A UNICEF/WHO report [2] states that 19 % of all deaths in children under five are due to pneumonia, the leading killer of children worldwide.

Tuberculosis is a lung disorder associated with high morbidity and mortality rates [3–5]. The mortality rate can be reduced by diagnosing them at an early stage. India accounts for one fifth of the global TB incident cases [6]. The lung disorder named bronchiectasis is a disorder of the bronchi of the lungs, characterized by permanent, abnormal dilation and destruction of bronchial walls. Its radiological features normally exist in the internal region of the lung parenchyma.

However, there is a chance that the radiologists miss diagnosis because of the small size of bronchiectasis nodules at an early stage. Early diagnosis of lung disorders has become possible with the tremendous growth of imaging technology and information processing techniques which has led to the development of computer-aided diagnostic (CAD) systems to assist the radiologist in performing better diagnosis. A CAD system is one which is capable of analyzing the data related to the patient under investigation and suggesting a diagnosis based on the analysis. In our work the data is in the form of CT images of the chest and hence image analysis is done to perform diagnosis.

As with many image analysis system, segmentation plays an integral role in the CAD system developed for diagnosis of lung disorders. The success of the other components of an image analysis system depends on the accuracy of the segmentation subsystem. This is especially true with a computer-aided diagnosis system that analyzes the chest CT image to detect any lung disorders. If the segmentation subsystem does not segment the lung parenchyma completely there is a chance of the CAD system missing a few pathology-bearing regions (PBRs). This happens in cases where a part of the lung parenchyma is segmented with the outer chest due to similar pixel values in peripheral PBRs and the outer chest region. Hence, it is very important that the segmentation result is accurate.

Conventional methods for lung segmentation rely on the difference in pixel intensities between the lung and surrounding tissues. According to Sluimer et al. [7], segmentation of lungs in presence of pathology continues to be one of the biggest challenges in medical image analysis. Lai and Ye [8] state that segmentation of lungs is affected by high-density pathologies that are connected to the lung border and that discontinuities in the pixel intensities may be caused by X-ray projecting intensity changes, differing tissue reflectance, and transmission properties, so the conventional segmentation does not give good results. They also specify that presence of juxta-pleural nodules at the margin of chest wall may result in inaccurate segmentation and that the rolling ball algorithm used by some authors has the problem of fixing the size of the structuring element used in morphological operations. They also state that the problem that has not yet been solved is the segmentation of lungs affected by high-density pathologies that are connected to the lung border. They conclude that a segmentation algorithm developed for a specific type of image will not be suitable for segmenting other types of images. Hence many of the existing approaches are not suitable for segmentation of lung CT image with any type of pathology.

Tuberculosis and pneumonia are two major lung disorders in which the PBR is large and peripherally placed. For computer analysis such as detection and quantification of abnormal areas, it is vital that the complete lung part of the image is extracted by the segmentation approach used in the system.

The rest of the paper is organized as follows: Section “Literature Survey” provides a survey of literature existing in lung

segmentation. Section “Materials and Methods” discusses the implementation details of the work. Section “Experimental Results” presents the experimental results. Section “Conclusion and Future Enhancement” presents the conclusion derived from the work and the enhancements that can be carried out in future.

Literature Survey

Hu et al. [9] in their work have presented a fully automatic method for identifying the lungs in three-dimensional (3D) pulmonary X-ray CT images. The method involves three main steps namely, optimal thresholding, separation of the left and right lungs, and a sequence of morphological operations. Optimal thresholding is first applied to extract the lung region from the CT images. Then dynamic programming is applied to separate the left and right lungs by identifying the anterior and posterior junctions. Finally, a sequence of morphological operations is used to smooth the irregular boundary along the mediastinum. They have tested their method by processing 3D CT data sets from eight normal subjects, each imaged three times at biweekly intervals with lungs at full inspiration. They have compared the automatic method to manually traced borders from two image analysts. Averaged over all volumes, the root mean square difference between the computer and human analysis is found to be 0.8 pixels (0.54 mm). From the literature it is found that the approach was tested only using healthy chest CT images but was not tested using images with pathology. It is evident that the approach will not produce the complete lung if tested with images with severe pathology and hence is not suitable for CAD systems for diagnosis of diseases like tuberculosis and pneumonia in which the PBR is on the periphery.

Khawaja et al. [10] have proposed a method for the segmentation of lung from chest CT. The method consists of three phases, namely, enhancement of lung CT, elliptical thorax extraction, and lungs segmentation. In the proposed approach, they have utilized the fact that the pleural membrane forms the distinguishing boundary between the lung and its surroundings. The segmentation algorithm was tested on 964 slices, belonging to six benign and three malignant cases. They claim that the proposed method of lungs segmentation performs efficiently not only on chest CT without any pathology, but also works equally well on images containing abnormality patches and nodules in any part of the lung. But our experimentation shows that elliptical thorax extraction may not work in all cases. This is because the shape of the lung in all the CT slices is not perfectly elliptical.

Sluimer et al. [7] in their work have proposed a segmentation-by-registration scheme for segmentation of lung from chest CT in which an atlas-based segmentation of the pathological lungs is refined by applying voxel classification to the border volume of the transformed

probabilistic atlas. They have compared the performance of the proposed approach and three other segmentation methods, namely, a conventional lung field segmentation based on thresholding and morphological techniques, a conventional segmentation employing user interaction and a voxel classification method. For their comparative study they have chosen a dataset of 10 scans that are difficult to segment by conventional methods. They have used the three measures, namely, volumetric overlap fraction, Hausdorff distance (or maximum surface distance), and mean absolute surface distance for evaluation against manual segmentations. They have inferred four results: (1) “The automatic region growing method was unable to adequately segment the pathological test scans.”, (2) “In segmenting high-density tissues, both voxel classification and refined segmentation-by-registration outperformed the manually aided region growing method.”, (3) “Refined segmentation-by-registration achieved a significant improvement upon straightforward segmentation-by-registration results.”, and (4) “None of the tested methods approached the performance of the second observer in segmenting the most pathological scan.”. They also state that accurate lung segmentation in the presence of PBR attached to the pleura is not possible using conventional methods based on thresholding and morphological processing, and that the segmentation of pathological scans requires a different approach than the segmentation of normal scans. They add that the interactive approach achieves better overall segmentation results than the fully automatic region growing method. They claim that the registration scheme has the desirable property of automatically creating segmentations with a valid lung shape due to its implicit lung model. From their experimental results they infer that the refined segmentation-by-registration scheme performs well on scans with up to a quarter of the lung volume affected by high-density pathology and state that the method should be tested on a larger amount of scans before it can be reliably deployed in clinical practice. They conclude that for more severely pathological scans, the accuracy achieved is still unsatisfactory.

Chen et al. [11] in their work have proposed a method for automatic pulmonary parenchyma segmentation in CT images. They have used a mid-value nonlinear filter for noise removal. Thresholding is then applied to the denoised image to segment the lung regions from the whole CT image. Region flood filling has been used to remove artifacts outside the lung. Isolated artifacts are then removed by applying morphological operations and area filter. Finally, the obtained binary image is used as a mask to the original CT slice to extract the pulmonary parenchyma. They have evaluated the scheme using a sequence of 75 CT image slices. From the experimental results they conclude that the method is simple and easily implemented with little algorithmic complexity. They claim that the proposed

method is efficient enough to be used as an initial step to lung disease CAD system based on CT images but have not discussed the experimental results in case of images with peripherally placed pathologies.

Lai and Ye [8] have proposed an active contour-based lung field segmentation approach with prior knowledge about shape to fit the lung boundary. It fully exploits the available a priori knowledge concerning the anatomic structure of interest. They claim that it can be used in pulmonary regions of arbitrary shape, and is especially suitable for the segmentation of lung field with juxta-pleural pulmonary nodules due to fitting with the shape profile for pulmonary area.

Elizabeth et al. [12], in their work have developed a CAD system for diagnosis of bronchiectasis. The developed system efficiently detects the images of patients diseased by bronchiectasis and classifies according to the severity conditions. The system was able to differentiate bronchiectasis from other diseases and hence perform efficiently even when tested with images having other lung disorders. However, it was found that segmentation of lung parenchyma would be a challenging task in the presence of peripherally placed PBRs. This was not an issue in case of CT images affected by bronchiectasis. In their next work [13], an automated approach to segmentation of lung parenchyma from the chest CT image was presented. The approach involves the conventional optimal thresholding technique, and operations based on convex edge and centroid properties of the lung region. Though the segmentation approach proposed in this work improved the diagnostic performance of the CAD system, it was still not capable of segmenting lungs with peripheral PBRs with a major portion of the lung bearing the pathology. Hence this work aimed at solving the problem of handling segmentation in images with peripherally placed PBRs.

From the literature discussed in this section on segmentation approaches that can be used in CAD systems for diagnosis of lung disorders, it can be inferred that thresholding approach is incapable of segmenting the lung correctly in the presence of peripheral PBR. Registration also becomes expensive due to the fact that lung volume varies with respect to several factors and the lung shape differs between slices.

Compared to the works discussed in the literature the work discussed in this paper is different in the following ways: our work attempts to reconstruct the lung with peripheral PBR. This is achieved by using the right lung as the template if the left lung bears a peripheral PBR and the left lung as template if the right lung bears a peripheral PBR. The proposed approach is suitable for segmentation of normal lungs and lungs with severe pathology attached to the borders. Some additional region may be segmented together with the lung parenchyma in a few cases; but it does not miss any peripheral PBRs and the additional regions

produced are eliminated by the classifier. The proposed approach does not require a database of templates for reconstruction of the severely affected lung as it uses the shape properties of the lung which is completely segmented. The corresponding lung from an atlas could have been used as a template, provided, the atlas takes into account the factors that influence the volume and hence the area of the different slices of the lung. Registration becomes expensive due to the fact that lung volume varies with respect to several factors [14–16] and the lung size and shape differs between slices. Hence, in this work to reconstruct the convex border of the lung with severe pathology, the other lung from the same slice is used. The result of this segmentation procedure is not symmetric lung. Instead, due to reflection and translation, the convex border is reconstructed and the pixel intensities of the original lung tissue are used to obtain the lung tissue. Hence, the difference in the number of lobes and the size between the two lungs is still retained.

Materials and Methods

The architecture of the CAD system that has been developed to detect lung disorders, namely bronchiectasis, tuberculosis, and pneumonia is shown in Fig. 1. The CAD system is composed of two major components the training subsystem and inference subsystem.

In the training subsystem, the chest CT images in the dataset (T-1) are processed by noise filtering, edge enhancement, segmentation, and region of interest (ROI) extraction. Features are then extracted from the ROIs and stored in the image database.

These feature vectors (T-5) and the corresponding diagnosis given by an expert are used to train a backpropagation neural network (BPNN). Rules are extracted from the trained neural network and stored in the knowledge base (KB) along with the feature vectors and corresponding diagnosis (T-6). The trained BPNN and KB can now be used for diagnosis of a chest CT.

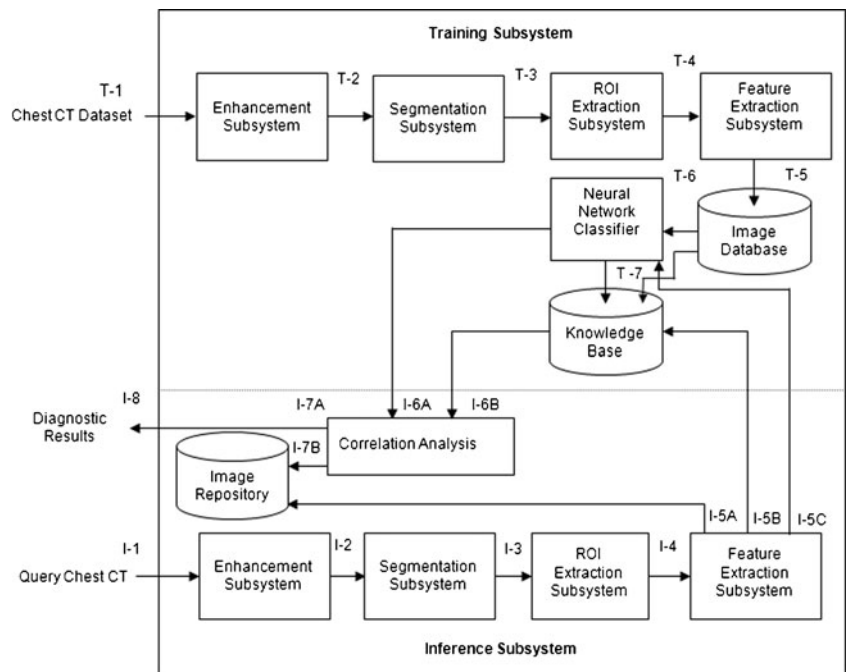
When a query image (I-1) is given to the inference subsystem, it is processed by noise filtering, segmentation, and ROI extraction. The features of the individual ROIs (I-4) are extracted by the feature extraction subsystem and the extracted features are given as input to the trained BPNN. It is also used to query the KB. The classification given by the BPNN and the inference given by the KB are then correlated and the diagnostic results are determined.

An image repository is maintained to store the feature vectors and the corresponding diagnosis after processing each query image. The content of the image repository is transferred to the image database after processing of every 100 images. The neural network (NN) is trained and the KB is updated with every addition to the image database, thereby refining the NN and the KB. This improves the performance of the system in the long run. The training subsystem and the inference subsystem are explained in detail with the relevant algorithms in the following subsections.

Training Subsystem

The training subsystem is responsible for training the CAD system to perform correct diagnosis by teaching the system with labeled examples. The various components of the training subsystem are enhancement subsystem, segmentation

Fig. 1 System architecture



subsystem, ROI extraction subsystem, feature extraction subsystem, image database, neural network, and knowledge base.

Enhancement Subsystem

The main objective of the enhancement subsystem is to make the image more suitable for the subsequent subsystems to handle as compared to the original image. According to Hanson [17], it is the random noise in a CT image that ultimately limits the ability of the radiologist to discriminate between two regions of different density. Hence it is necessary to eliminate this noise. But such noise cannot be completely eliminated from the image because of its unpredictable nature and will always lead to some uncertainty in the interpretation of the image. He adds that there is strong evidence that much of the random noise in CT scanners is due to the statistical inaccuracies arising from the detection of a finite number of transmitted X-ray quanta. Random noise has Gaussian amplitude distribution. Adaptive Wiener filter [18], described by Eq. 3, is used for denoising because it is found to work best when the noise is constant-power additive noise, such as Gaussian noise. It tailors itself to the local image variance; in case of large variance, it performs little smoothing; where the variance is small, it performs more smoothing.

It estimates the local mean and variance around each pixel using Eqs. 1 and 2, respectively.

$$\mu = \frac{1}{NM} \sum_{n_1, n_2 \in \eta} a(n_1, n_2) \quad (1)$$

$$\sigma^2 = \frac{1}{NM} \sum_{n_1, n_2 \in \eta} a^2(n_1, n_2) - \mu^2 \quad (2)$$

where η is the N-by-M local neighborhood of each pixel in the image A.

Using these estimates a Pixelwise Wiener filter is created using Eq. 3.

$$b(n_1, n_2) = \mu + \frac{\sigma^2 - v^2}{\sigma^2} (a(n_1, n_2) - \mu) \quad (3)$$

where v^2 is the noise variance. If the noise variance is not given, it uses the average of all the local estimated variances.

In this application segmentation subsystem and ROI extraction subsystem would work effectively if the edges are sharp. Hence, a Laplacian filter [19], defined by Eq. 4, has been used to extract the edges and these edges have been superimposed on the denoised image.

$$g(x,y) = 5f(x,y) - [f(x+1,y) + f(x-1,y) + f(x,y+1) + f(x,y-1)] \quad (4)$$

where $f(x,y)$ is the denoised image, $g(x,y)$ is the Laplacian filtered image, and (x,y) are the spatial coordinates of the image.

A suitable weight is used for superimposing the edges, so that the chance of values exceeding the intensity range is avoided. The weight was chosen as 0.5 through experimentation and the superimposed image is defined by Eq. 5.

$$e(x,y) = f(x,y) + 0.5 \times g(x,y) \quad (5)$$

Segmentation Subsystem

Segmentation subsystem is responsible for extracting the lung parenchyma from the rest of the chest in the chest CT. The phases involved in the proposed segmentation algorithm are shown in Fig. 2.

The images are labeled to fall within two classes, completely segmented and incompletely segmented lung, based on the information given by a radiologist. A multilayer feed forward network comprising of four layers, namely, one input layer, two hidden layers and one output layer is created. The 26 features extracted in step 5 of process 5 in algorithm 1 correspond to the 26 nodes in the input layer. Eight nodes are used in the first hidden layer, four nodes in the second hidden layer and one node in the output layer. The number of layers and the number of nodes in the hidden layers was determined after several experimentations. The network was trained using backpropagation algorithm with 183 images, 150 from class 0 (correctly segmented), and 33 from class 1 (incompletely segmented). The trained neural network is capable of classifying the segmented image between the two classes. If any of the images is classified as belonging to class 1, the lung borders are reconstructed. The detailed algorithm used for segmentation is shown in Algorithm 1.

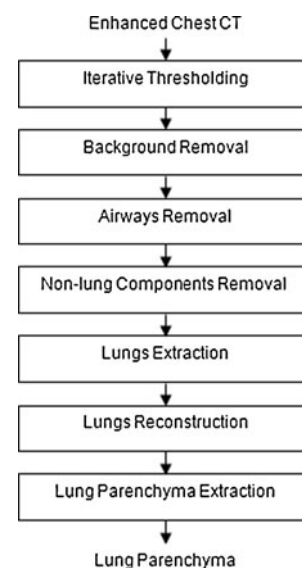


Fig. 2 Phases of segmentation subsystem

Algorithm 1: Algorithm for segmentation of lung parenchyma

Process 1: Iterative thresholding [20]

Input:

Enhanced chest CT

Process logic:

Step 1: Global image threshold is computed using Otsu's method [21]. It is used as the initial threshold.

Step 2: The pixels with grayscale value less than threshold are set to 0 and pixels with grayscale value greater than or equal to threshold are set to 1.

Step 3: The mean grayscale value of pixels set to 0 is determined.

Step 4: The mean grayscale value of pixels set to 1 is determined.

Step 5: The average of the means obtained in steps 3 and 4 is chosen as the threshold for the next iteration.

Step 6: Iterate from step 2 until the threshold converges to the threshold of the previous iteration.

Output:

Thresholded image

Process 2. Background removal

Input:

Thresholded image

Process logic:

Step 1: The thresholded image is complemented.

Step 2: The white pixels connected to the border are set to 0 [22].

Output:

Binary image with the outer chest region removed.

Process 3. Airways removal

Input:

Binary image with the outer chest region removed.

Process logic:

Step 1: The white pixels that are not connected to the border are set to 0. This removes the airways.

Output:

Binary image with holes formed by airways removed.

Process 4. Non-lung components removal

Input:

Binary image with holes formed by airways removed.

Process logic:

Step 1: The small connected components in the outer chest region are removed.

Step 2: The connected components with an eccentricity greater than 0.98 in the outer chest region are removed because lungs would have lesser eccentricity which means that lungs are more circular as compared to objects with an eccentricity of 0.98.

Output:

Binary image with external components in the chest region removed.

Process 5. Lungs extraction

Input:

Binary image with external components in the chest region removed.

Process logic:

Step 1: The connected components are labeled based on eight-connectivity and the number of connected components is determined.

Step 2: If number of connected components is greater than 2, the two largest connected components are set to 1 and the other pixels are set to 0; the pixels which are set to one form the pixel positions corresponding to the parenchyma.

Step 3: If the number of connected components is 2,

- a. If the area of the largest connected component is greater than 30,000, the two lungs are connected and form a single component and the other component is a non-lung component. Hence retain the largest component alone and go to step 4; else go to step 5.

Step 4: If the number of connected components is 1

- a. Lung junction is identified.
- b. Local thresholding is applied to the lung junction.
- c. Morphological close operation is performed.

Step 5: The shape features namely, MajorAxis Length, MinorAxis Length, Eccentricity, ConvexArea, EquivDiameter, Solidity, Extent, Centroid, BoundingBox, Area of the left lung to that of the right lung, and ratio of the Perimeter are extracted from each of the two lungs are extracted

and a feature vector of size 26, comprising of the MajorAxis Length, MinorAxis Length, Eccentricity, ConvexArea, EquivDiameter, Solidity, and Extent of each lung, Centroid of the left lung–Centroid of the right lung, BoundingBox of the left lung–BoundingBox of the right lung, BoundingBox, ratio of the Area of the left lung to that of the right lung and ratio of the Perimeter of the left lung to that of the right lung is constructed. These features are computed as stated in steps 5a through 5k.

- a. MajorAxis Length is computed as the number of pixels along the major axis of the ellipse that has the same normalized second central moments as the lung.
- b. MinorAxis Length is computed as the number of pixels along the minor axis of the ellipse that has the same normalized second central moments as the lung.
- c. Eccentricity is computed as the eccentricity of the ellipse that has the same second-moments as the lung. The eccentricity is the ratio of the distance between the foci of the ellipse and its major axis length.
- d. ConvexArea is computed as the number of pixels in Convex Image of the lung; Convex Image is a binary image with all pixels within the hull filled in; Convex hull is the smallest convex polygon that can contain the lung.
- e. EquivDiameter is computed as the diameter of a circle with the same area as the lung and is defined by $\text{Equivdiameter} = \sqrt{\frac{4 \times \text{Area}}{\pi}}$
- f. Solidity is computed as the proportion of the pixels in the convex hull that are also in the lung and is defined by $\text{Solidity} = \frac{\text{Area}}{\text{ConvexArea}}$
- g. Extent is computed as the proportion of the pixels in the bounding box that are also in the lung and is defined by the ratio of the Area of the lung to the area of the bounding box.
- h. Centroid is computed as the center of mass of the lung.
- i. BoundingBox is computed as the smallest rectangle containing the lung.
- j. Area is computed as the actual number of pixels in the lung.
- k. Perimeter is computed as the distance around the boundary of the lung.

Step 6: The extracted features are fed as input to a trained feed forward back propagation neural network.

Step 7: If the output of the neural network is 0, go to process 7.

Step 8: If the output of the neural network is 1, the severely affected lung is reconstructed using process 6.

Output:

Binary image of the segmented lungs, either complete or incomplete.

Process 6: Lungs reconstruction

Input:

Binary image of incompletely segmented lungs.

Process logic:

Step 1: Find the height of each lung.

Step 2: The lung which has lesser height is considered to be the severely affected one.

Step 3: The pixel coordinates of the other lung which is healthy or less affected are taken and reflected to get a symmetric lung in place of the severely affected lung.

Step 4: In order to cater to the difference in separation between the two lungs in case of the reflected lung and the original lung.

- a. The severely affected lung is segmented from the incomplete lung parenchyma.
- b. The relative position of the lung from the centre of the image along the horizontal (y) direction is determined.
- c. The reflected image is translated to the position obtained in step 4 b. This gives the pixel positions corresponding to the parenchyma.
- d. Pixelwise logical OR is performed between the output of process 5 and the output of step 4 c in process 6.
- e. The resultant image is smoothed by performing dilation and erosion.

Output:

Binary image consisting of the two lungs.

Process 7: Lung parenchyma extraction

Input:

Binary image consisting of the two lungs

Process logic:

Fill the pixel positions of the lung parenchyma by the pixel values in the input chest CT.

Output:

Lung parenchyma

ROI Extraction Subsystem

The goal of ROI extraction subsystem is to extract the ROIs from the lung parenchyma. The ROIs of this system are the regions expected to bear the pathologies. The ROIs are

extracted by the region growing algorithm [19]. The PBRs and bronchial walls are associated with high-intensity values and the normal lung tissues have low-intensity values. Hence two seed points are chosen in such a way that one corresponds to high intensity and the other corresponds to

low intensity. Each pixel in the lung parenchyma is analyzed for its proximity to the seed points and is labeled with either 0 or 1 based on whether it is close to the low-intensity seed point or the high-intensity seed point, respectively. The regions formed are tested for connectivity and are labeled using the algorithm proposed by Rosenfeld and Pfaltz [23]. The regions other than these ROIs are removed by morphological operations.

Feature Extraction Subsystem

The shape and texture features of the extracted ROIs are determined for quantitative analysis of the regions. Area, Euler number, extent, perimeter, solidity, eccentricity, orientation, elongation, and form factor of each ROI were computed. The histogram of each ROI was generated and the first five moments were computed. Gray level co-occurrence matrix (GLCM) was created for each ROI. GLCM is defined as a matrix of relative frequencies, $p(i, j)$ with which two neighboring pixels separated by distance, d at a specified angle, θ occur on the image, one with gray level, i , and the other with gray level, j . Once the GLCMs were calculated along each direction, several texture descriptors [24, 25], namely contrast, correlation, energy, homogeneity, dissimilarity, entropy, inverse difference moment, and diagonal moment were calculated to capture the texture properties and differentiate among regions with different textures. In addition the mean, variance, entropy, and the same eight features from GLCM of the approximations of the level 2 wavelet decomposition of each ROI were computed.

Area is the actual number of pixels in the ROI. Euler number is the number of objects in the region minus the number of holes in those objects. Extent is the proportion of the pixels in the bounding box that are also in the lung and is defined by the ratio of the area of the lung to the area of the bounding box; bounding box is computed as the smallest rectangle containing the ROI. Perimeter is computed as the distance around the boundary of the lung. Solidity is computed as the proportion of the pixels in the convex hull that are also in the lung and is defined by

$$\text{Solidity} = \frac{\text{Area}}{\text{ConvexArea}} \tag{6}$$

Eccentricity is computed as the eccentricity of the ellipse that has the same second-moments as the lung. The eccentricity is the ratio of the distance between the foci of the ellipse and its major axis length. Orientation is the angle between the x -axis and the major axis of the ellipse that has the same second-moments as the region. Elongation is defined by the ratio of the length to the width of the bounding box of the ROI. Form factor is defined by

$$\text{FormFactor} = \frac{4 \times \text{Area}}{\text{Perimeter}^2} \tag{7}$$

Contrast is a measure of image intensity or the local variations present in an image to show the texture fineness. Contrast is also known as variance and inertia and is defined by

$$\text{Contrast} = \sum_{i=1}^{N_g} \sum_{j=1}^{N_g} (i - j)^2 p(i, j) \tag{8}$$

Correlation is the measure of how a pixel is correlated to its neighbor over the PBR. It measures the linear dependency of the gray level values in the co-occurrence matrix or the correlation presenting along a scan line of an image and is defined by

$$\text{Correlation} = \frac{\sum_{i=1}^{N_g} \sum_{j=1}^{N_g} ij p(i, j) - \mu_{\text{col}} \mu_{\text{row}}}{\sigma_{\text{col}} \sigma_{\text{row}}} \tag{9}$$

where μ represents mean and σ represents standard deviation.

Energy, angular second moment, or uniformity, measures the image homogeneity. Homogeneity is the measure of closeness of the distribution of elements in the GLCM to the GLCM diagonal of each PBR and is defined by

$$\text{Homogeneity} = \sum_{i,j} \frac{p(i, j)}{1 + |i - j|} \tag{10}$$

Dissimilarity is used to measure the dissimilarity between two gray levels i and j and is defined by

$$\text{Dissimilarity} = \sum_{i=1}^{N_g} \sum_{j=1}^{N_g} |i - j| p(i, j) \tag{11}$$

Entropy is the opposite measure of angular second moment. This descriptor of randomness produces a low value for an irregular co-occurrence matrix. It is defined by

$$\text{Entropy} = - \sum_{i=1}^{N_g} \sum_{j=1}^{N_g} p(i, j) \log_2 p(i, j) \tag{12}$$

Inverse difference moment is defined by

Inverse difference moment

$$= \sum_{i=1}^{N_g} \sum_{j=1}^{N_g} \frac{1}{1 + (i - j)^2} p(i, j) \tag{13}$$

Diagonal moment is defined by

$$\text{Diagonal moment} = \sum_{i=1}^{N_g} \sum_{j=1}^{N_g} \sqrt{0.5|i - j|} p(i, j) \tag{14}$$

where N_g is the maximum gray level.

Mean is the measure of average intensity of the PBR and is defined by

$$\text{Mean} = \sum_{i=0}^{L-1} z_i p(z_i) \quad (15)$$

Variance is the measure of average contrast of each PBR and is defined by

$$\sigma = \sum_{i=0}^{L-1} (z_i - m)^2 p(z_i) \quad (16)$$

Entropy is the measure of the randomness of intensity in each PBR and is defined by

$$\text{Entropy} = - \sum_{i=0}^{L-1} p(z_i) \log_2 p(z_i) \quad (17)$$

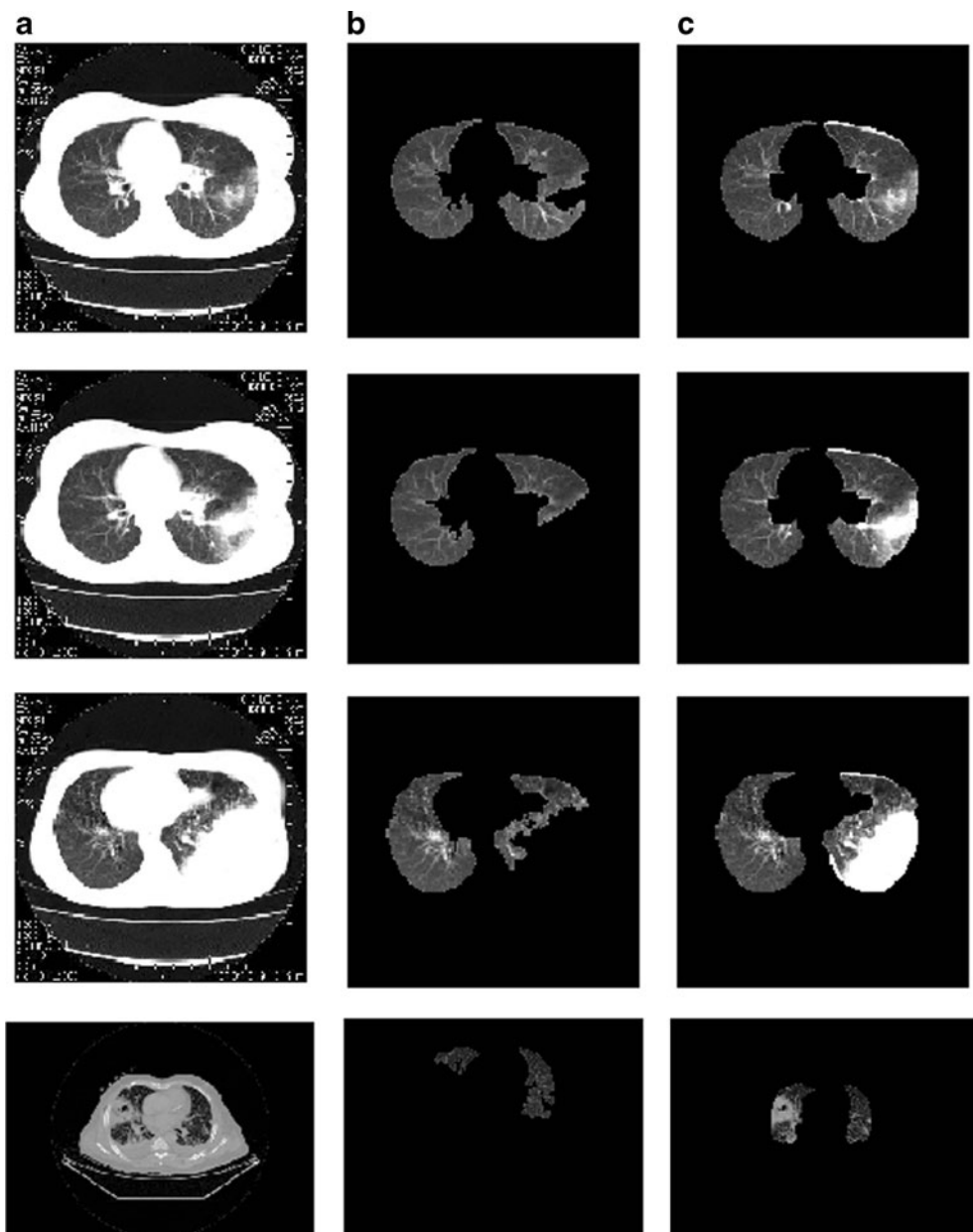
where L is the number of gray levels, z_i is the i th gray level.

Image Database

The image database is created using Oracle 10 g and organized as two relations:

IMAGE (ImageID, Image) and
 FEATURES (ROIID, Area, EulerNumber, Extent, Perimeter, Solidity, Eccentricity, Orientation, Elongation, FormFactor, Moment1, Moment2, Moment3, Moment4, Moment5, SpContrast, SpCorrelation, SpEnergy,

Fig. 3 Results of segmentation. **a** Input image. **b** Segmentation by thresholding. **c** Segmentation by proposed approach



SpHomogeneity, SpDissimilarity, SpEntropy, SpIDM, SpDiagonalMoment, W1Mean, W1Variance, W1Entropy, W1Contrast, W1Correlation, W1Energy, W1Homogeneity, W1Dissimilarity, W1EntropyGLCM, W1IDM, W1DiagonalMoment, W2Mean, W2Variance, W2Entropy, W2Contrast, W2Correlation, W2Energy, W2Homogeneity, W2Dissimilarity, W2EntropyGLCM, W2IDM, W2DiagonalMoment, Image ID), where the attributes with the prefix Sp represent the features extracted from the spatial domain, the attributes with the prefix W1 represent the features extracted from the approximation of the level 1 wavelet decomposition and the attributes with the prefix W2 represent the features extracted from the approximation of the level 2 wavelet decomposition. The primary key of the relation, IMAGE is ImageID. The data type for ImageID is VARCHAR(15). Image is stored in BLOB format. The primary key of the relation FEATURES is {ROIID, ImageID}. Image ID in the relation FEATURES references the IMAGE relation. The data type of ROIID is NUMBER(3) and that of the features is NUMBER(13, 8).

Neural Network

A multilayer neural network (NN) was created for diagnosis of lung disorders based on the features extracted by the feature extraction subsystem. The NN used in our work consists of 44 nodes in the input layer, 32 nodes in the hidden layer, and four nodes in the output layer. The number of input units was chosen equal to the number of features extracted from each ROI. The number of hidden units was selected after sufficient analysis. The four output units correspond to class 0, class 1, class 2, and class 3, which

represent healthy region, bronchiectasis-affected region, tuberculosis-affected region, and pneumonia-affected region, respectively. The NN was trained using Backpropagation algorithm with the data stored in the image database and the labels assigned to the ROIs by an expert.

Knowledge Base

The knowledge base is constructed using the dataset used for training and the outputs produced by the trained NN for the training dataset. It is composed of facts and rules. Facts are the feature vectors used for training together with the corresponding diagnosis. Rules are generated based on the outputs of the trained NN for the training dataset.

Inference Subsystem

The goal of the inference subsystem is to generate diagnostic results. The inference subsystem comprises enhancement subsystem, segmentation subsystem, ROI extraction subsystem, feature extraction subsystem, trained neural network, knowledge base, and correlation analysis.

When a chest CT is given to this subsystem, it first preprocesses the image by performing enhancement, segmentation, ROI extraction, and feature extraction as discussed in Sections “Enhancement Subsystem” through “Feature Extraction Subsystem”. The features extracted from each ROI are fed to the trained NN and the KB, each of which classifies the ROI as belonging to one of the four classes considered. The final diagnostic result is determined based on the correlation between the classification result provided by the NN and inference provided by the KB.

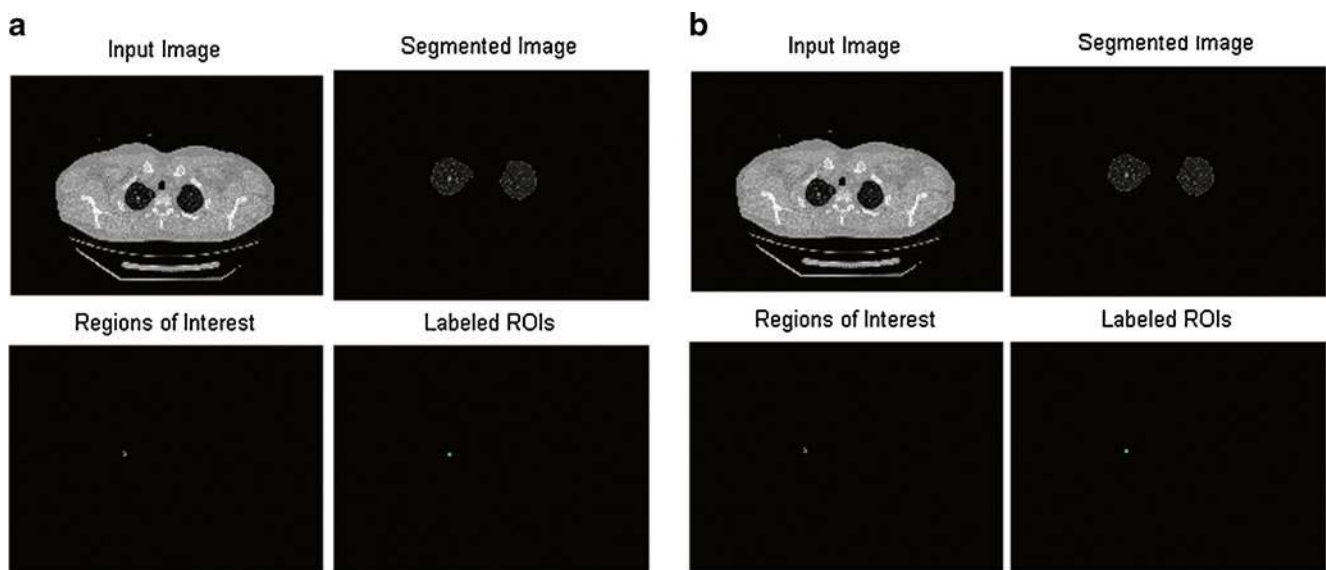


Fig. 4 **a** Results obtained for an image of a patient with mild bronchiectasis using thresholding and morphological operations (number of ROIs=1). **b** Results obtained for an image of a patient with mild bronchiectasis using the proposed approach (number of ROIs=1)

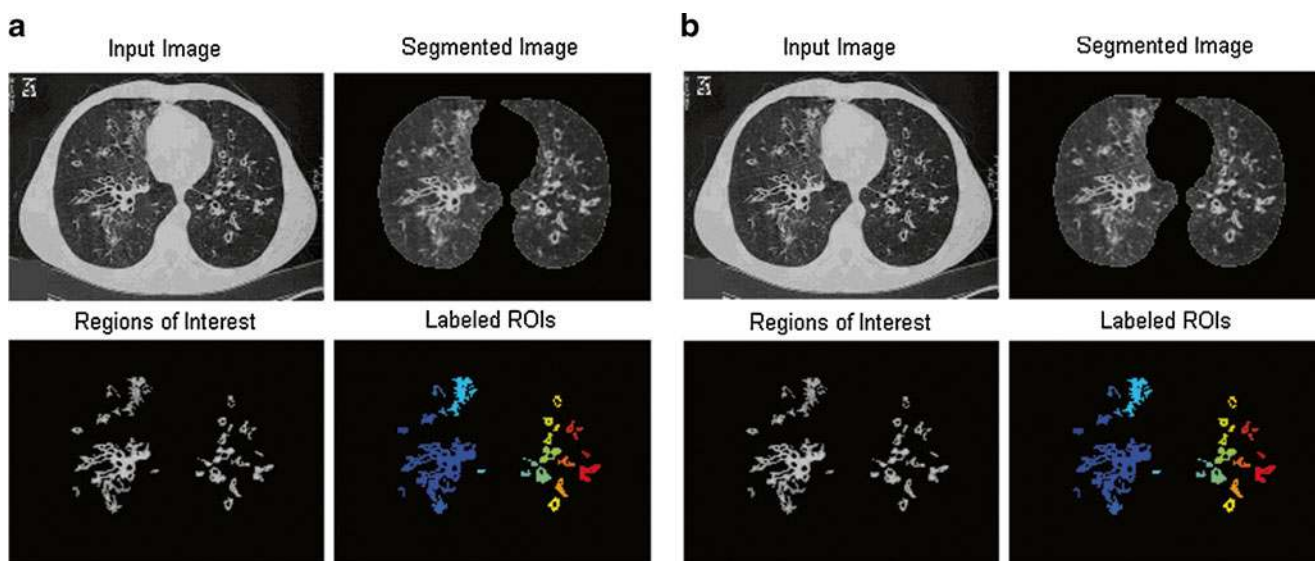


Fig. 5 **a** Results obtained for an image of a patient with severe bronchiectasis using thresholding and morphological operations (number of ROIs=19). **b** Results obtained for an image of a patient with severe bronchiectasis using the proposed approach (number of ROIs=19)

Correlation Analysis

Pearson's correlation coefficient (invented by Karl Pearson) is computed between the output of the NN and the output of the KB. The output from the neural network is a vector of size 4, the value of each lying between 0 and 1. Hence the inference given by the KB is also converted to a vector of size 4, each corresponding to a specific class, by setting the value to 1, in case the inference corresponds to that class.

Finally, the outputs from the NN, the KB, and the correlation between the two are presented to the radiologist. This aids the radiologist in performing better diagnosis.

Image Repository

An image repository is maintained to store the details of every processed query image. It is organized in a way similar to the image database. After processing 100 images, the content of the image repository is transferred and added to the image database; the NN is trained again with the original data in the image database and the newly added data; the KB is updated. This helps in improving the performance of the system further as the collection in the image database increases. At one stage, there could be a problem of overtraining, which should be handled. This can be handled by eliminating the outliers

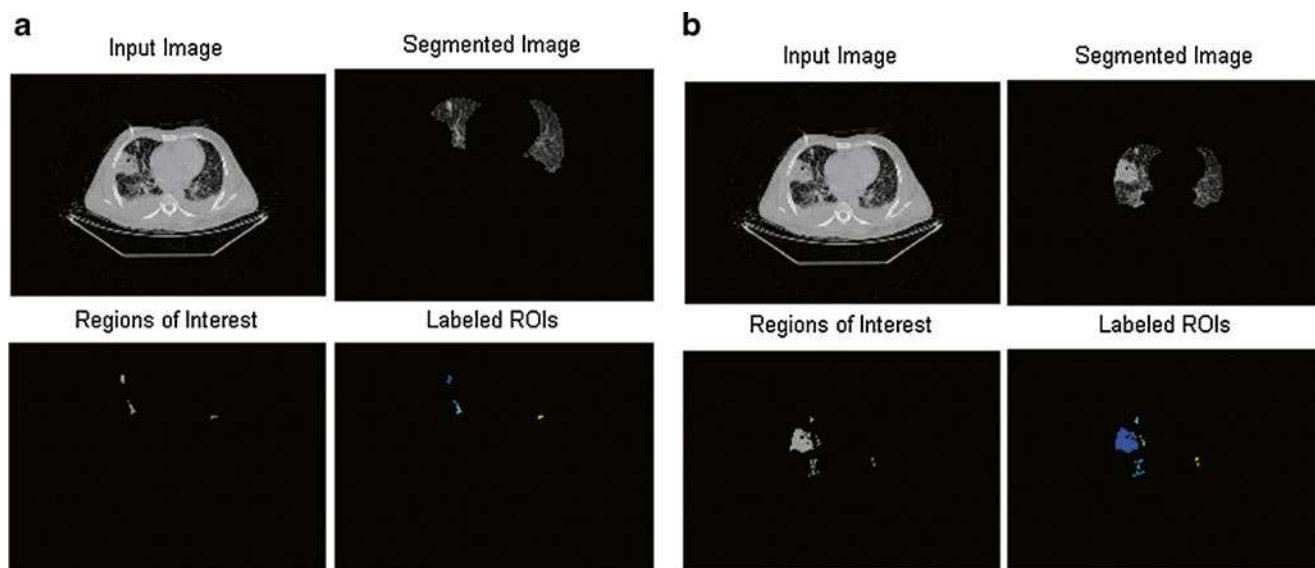


Fig. 6 **a** Results obtained for an image of a patient with TB using thresholding and morphological operations (number of ROIs=3). **b** Results obtained for an image of a patient with TB using the proposed approach (number of ROIs=6)

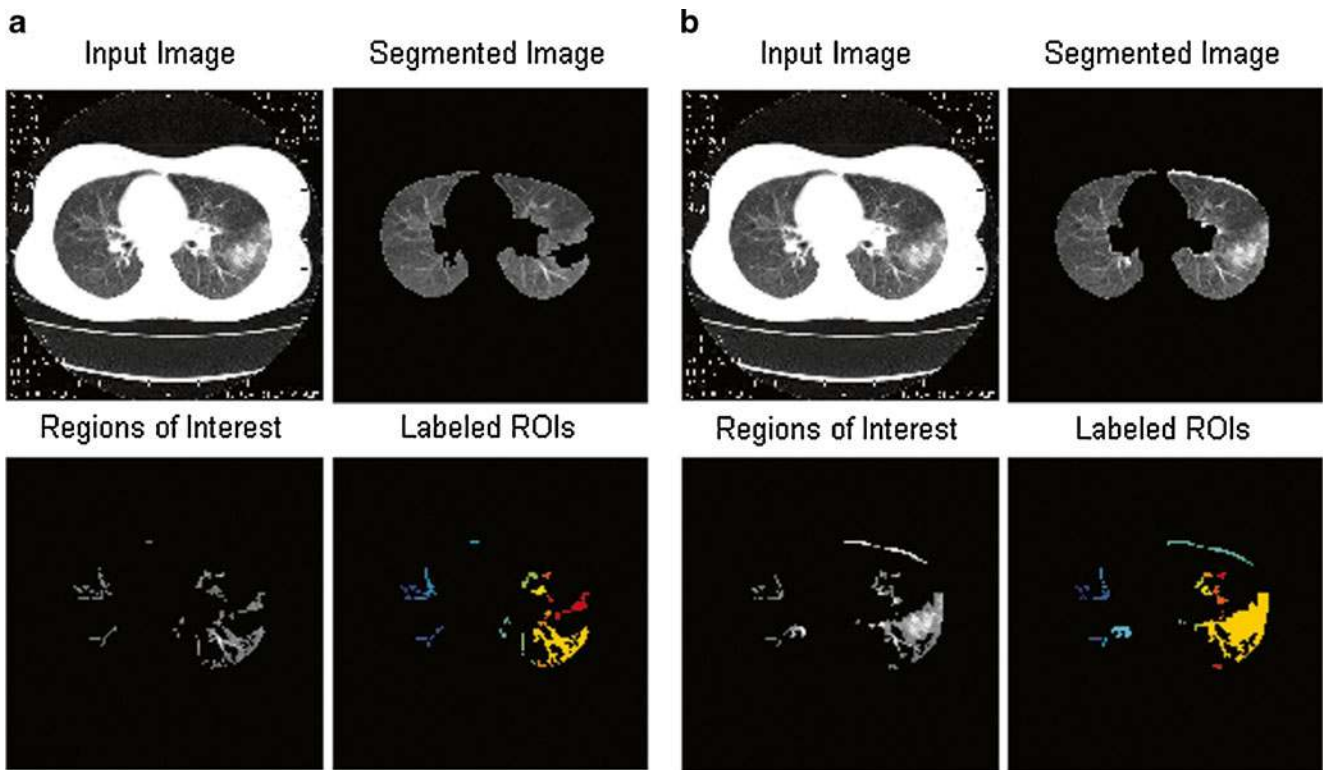


Fig. 7 **a** Results obtained for an image of a patient with pneumonia using thresholding and morphological operations (number of ROIs=21). **b** Results obtained for an image of a patient with pneumonia using the proposed approach (number of ROIs=19)

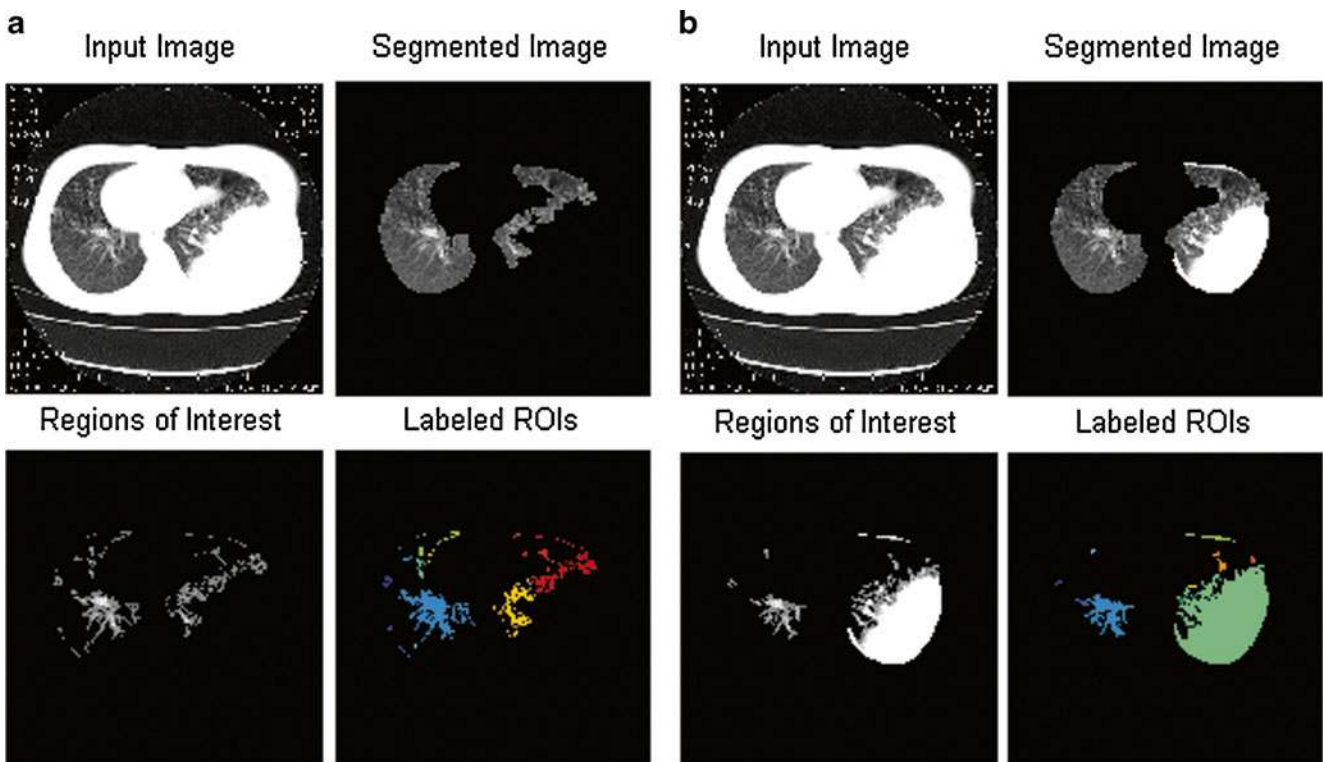


Fig. 8 **a** Results obtained for an image of a patient with pneumonia using thresholding and morphological operations (number of ROIs=20). **b** Results obtained for an image of a patient with pneumonia using the proposed approach (number of ROIs=9)

Table 1 Results obtained for 10-fold cross-validation

Fold	Accuracy	Specificity	Precision	Recall
Class 0				
Fold 1	100	100	100	100
Fold 2	100	100	100	100
Fold 3	96.77	92.86	94.44	100
Fold 4	100	100	100	100
Fold 5	90	95	94.44	85
Fold 6	100	100	100	100
Fold 7	100	100	100	100
Fold 8	100	100	100	100
Fold 9	94.29	94.74	93.75	93.75
Fold 10	71.43	57.89	70.37	82.61
Average	95.25	94.05	95.3	96.14
Class 1				
Fold 1	100	100	100	100
Fold 2	100	100	100	100
Fold 3	100	100	100	100
Fold 4	100	100	100	100
Fold 5	92.5	97.06	80	66.67
Fold 6	100	100	100	100
Fold 7	100	100	100	100
Fold 8	100	100	100	100
Fold 9	94.29	95.45	92.31	92.31
Fold 10	83.33	90.63	66.67	60
Average	97.01	98.31	93.9	91.9
Class 2				
Fold 1	97.5	96.97	87.5	100
Fold 2	100	100	100	100
Fold 3	96.77	100	100	88.89
Fold 4	100	100	100	100
Fold 5	92.5	90.91	70	100
Fold 6	100	100	100	100
Fold 7	100	100	100	100
Fold 8	100	100	100	100
Fold 9	100	100	100	100
Fold 10	100	100	100	100
Average	98.68	98.79	95.75	98.89
Class 3				
Fold 1	97.5	100	100	50
Fold 2	100	100	100	100
Fold 3	100	100	100	100
Fold 4	100	100	100	100
Fold 5	100	100	100	100
Fold 6	100	100	100	100
Fold 7	100	100	100	100
Fold 8	100	100	100	100
Fold 9	100	100	100	100
Fold 10	88.1	97.06	80	50
Average	98.56	99.71	98	90

determined by clustering and then by stopping the addition of training examples when the performance starts degrading with cross-validation.

Experimental Results

The image database used by our system consists of 400 ROIs extracted from 50 images, consisting of 20 bronchiectasis-affected CT images, 20 tuberculosis-affected CT images, and 10 pneumonia-affected CT images. The images are of size 512×512 . Figure 3 shows the results of segmentation; column (a) shows a subset of the input images, column (b) shows the two lungs obtained as a result of thresholding followed by morphological operations, and column (c) shows the results obtained by the proposed approach. The improvement in performance is observable since the complete lung is not segmented in case of segmentation by thresholding.

The ROIs extracted by the system using thresholding and the proposed segmentation algorithm are shown in Figs. 4, 5, 6, 7, and 8 for a subset of images; distinct connected components that form distinct ROIs are shown in different color for better visualization (color is indicated in online version only). The improvement in diagnosis is clear in cases where the PBR is peripherally placed, as shown from Figs. 6, 7, and 8. In cases of images where the PBRs are located internally, the proposed approach works equivalent to that of the thresholding technique, as shown in Figs. 4 and 5.

The CAD system was subject to 10-fold cross-validation and the results are tabulated in Table 1. The average performance measures are tabulated in Table 2.

It was not possible to perform an effective comparison with the equivalent system without the reflection step because with that approach, the ROI was either not detected or the ROI was detected as many very small ROIs instead of a single large size ROI in cases of lungs affected by tuberculosis and those affected by pneumonia, as is obvious from Figs. 6, 7, and 8. However, in case of lungs affected by bronchiectasis, the segmentation result, the ROIs extracted, and hence the diagnosis of the proposed system and the system without the reflection step were the same, as shown in Figs. 4 and 5.

Table 2 Summary of the results

	Accuracy	Specificity	Precision	Recall
Class 0	95.25	94.05	95.30	96.14
Class 1	97.01	98.31	93.90	91.90
Class 2	98.68	98.79	95.75	98.89
Class 3	98.56	99.71	98.00	90.00
Average	97.37	97.71	95.74	94.23

Conclusion and Future Enhancement

We have developed a CAD system for diagnosis of three lung disorders, namely, bronchiectasis, tuberculosis, and pneumonia. The performance of the system has been improved by a novel segmentation approach. The proposed approach first performs optimal thresholding and then makes use of a BPNN to determine if the segmented lung parenchyma is complete. If it is incomplete, the incomplete lung is reconstructed by using the other lung as template. In our study, patients with severe pathology in both the lungs were not examined. The approach could fail in such cases and in such cases segmentation by registration could be used with a compromise in complexity, because this requires a database of templates that takes into account the various factors that result in variation of the lung volume. The CAD system achieved an average accuracy of 97.37 %, specificity of 97.71 %, precision of 95.74 %, and recall of 94.23 %. The performance can be further improved by using the clinical test results as additional features. The segmentation process can be further improved by combining the concept of registration.

References

- World Health Organization. Tuberculosis. Fact sheet N°104 March 2010.
- UNICEF/WHO. Pneumonia: The forgotten killer of children. 2006.
- Greenaway C, Menzies D, Fanning A, Grewal R, Yuan L, FitzGerald JM: The canadian collaborative group in nosocomial transmission of tuberculosis: delay in diagnosis among hospitalized patients with active tuberculosis—predictors and outcomes. *Am J Respir Crit Care Med* 165:927–933, 2002
- van Well GTJ, Paes BF, Terwee CB, Springer P, Roord JJ, Donald PR, Furth AMV, Schoeman JF: Twenty years of pediatric tuberculous meningitis: a retrospective cohort study in the western cape of South Africa. *Pediatrics* 123:e1–e8, 2009
- Vree M, Huong NT, Duong BD, Sy DN, Van le N, Co NV, Cobelens FG, Borgdorff MW: Mortality and failure among tuberculosis patients who did not complete treatment in vietnam: a cohort study. *BMC Publ Health* 7:134, 2007
- World Health Organization. Global Tuberculosis Control: India. WHO REPORT 2009.
- Sluimer I, Prokop M, Ginneken BV: Toward automated segmentation of the pathological lung in CT. *IEEE Trans Med Imaging* 24:1025–1038, 2005
- Lai J, Ye M: Active contour based lung field segmentation. 2009 International Conference on Intelligent Human–Machine Systems and Cybernetics 2009, pp 288–291
- Hu S, Hoffman EA, Reinhardt JM: Automatic lung segmentation for accurate quantitation of volumetric X-ray ct images. *IEEE Trans Med Imaging* 20:490–498, 2001
- Khawaja MA, Aziz MZ, Iqbal N: Effectual lung segmentation for CAD systems using CT scan images. *Proceedings of IEEE, INMIC Conference* 2004. pp 49–54.
- Chen Z, Sun X, Nie S: An efficient method of automatic pulmonary parenchyma segmentation in CT images. *Proceedings of the 29th Annual International Conference of the IEEE EMBS Cité Internationale, Lyon, France* 2007. pp 5540–5542.
- Elizabeth DS, Kannan A, Nehemiah HK: Computer-aided diagnosis system for the detection of bronchiectasis in chest computed tomography images. *Int J Imaging Syst Technol* 19:290–298, 2009
- Elizabeth DS, Nehemiah HK, Raj CSR, Kannan A: A novel segmentation approach for improving diagnostic accuracy of CAD systems for detecting lung cancer from chest computed tomography images. *ACM Journal of Data and Information Quality* 3(2):4:1–4:16, 2012
- Garcia-Rio F, Dorgham A, Pino JM, Villasante C, Garcia-Quero C, Alvarez-Sala R: Lung volume reference values for women and men 65 to 85 years of age. *Am J Respir Crit Care Med* 180 (11):1083–1091, 2009
- Gupta CK, Mishra G, Mehta SC, Prasad J: On the contribution of height to predict lung volumes, capacities and diffusion in healthy school children of 10–17 years. *Indian J Chest Dis Allied Sci* 35 (4):167–77, 1993
- Bornstein BA, Cheng CW, Rhodes LM, Rashid H, Stomper PC, Siddon RL, Harris JR: Can simulation measurements be used to predict the irradiated lung volume in the tangential fields in patients treated for breast cancer? *Int J Radiat Oncol Biol Phys* 18(1):181–7, 1990
- Hanson KM: Noise and computed contrast discrimination in tomography, radiology of the skull and brain: Technical aspects of computed tomography, vol. 5, Chapter 113. C. V. Mosby, St. Louis, 1981, pp 3941–3955
- Wiener N: The Interpolation, Extrapolation and Smoothing of Stationary Time Series. NDRC Report, Cambridge. Wiley, New York, 1942
- Gonzalez RC, Woods RE: Digital Image Processing, 2nd edition. Prentice Hall Publications, New York, 2002
- Ridler TW, Calvard ES: Picture thresholding using an iterative selection method. *IEEE Trans Syst Man Cybern SMC-8:630–632*, 1978
- Otsu NA: Threshold selection method from gray-level histograms. *IEEE Trans Syst Man Cybern* 9:62–66, 1979
- Soille P: Morphological image analysis: principles and applications. Springer, New York, 1999, pp 164–165
- Rosenfeld A, Pfaltz JL: Sequential operations in digital picture processing. *J ACM* 13:471–494, 1966
- Haralick RM, Shanmugam K, Dinstein I: Textural features for image classification. *IEEE Trans Syst Man Cybern SMC-3:610–621*, 1973
- Haralick RM, Shapiro LG: Computer and robot vision. Addison-Wesley 1:460, 1992